# Computed tomography (CT)

Jiří Hozman, Jan Kybic

2005–2021

# Základní uspořádání systému CT

# CT history

- **1917** mathematical theory (Radon)
- **1956** tomography reconstruction in radioastronomy (Bracewell)
- **1963** CT reconstruction theory
- **1971** CT principles demonstrated (Hounsfield)
- **1972** first working CT for humans (EMI, London, Hounsfield)
- **1973** PET
- **1974** Ultrasound tomography
- **1982** SPECT
- **1985** Helical CT
- **1998** Multislice CT, 0.5 s/frame

# Johann Radon
**(matematik)**

*** 16.12.1887 Děčín, ČR**
**† 25.5.1956 Vídeň, Rakousko**

**1917 -** "Uber die Bestimmung von Funktionen durch ihre Integral-werte langs gewisser Mannigfaltigkeiten", *Berichte Sachsische Akademie der Wissenschaften. Leipzig, Math.-Phis. Kl.*, v.69, pp. 262-267. V této práci pan Radon matematicky vyřešil rekonstrukci prostorového obrazu na základě znalosti jeho projekcí.

# Sir Godfrey Newbold Hounsfield

1919-2004

Nottinghamshire, samouk, nenavštěvoval univerzitu
Nobelova cena 1979

## *Sir Godfrey Hounsfield*
## *Nobel Prize in Medicine, 1979*

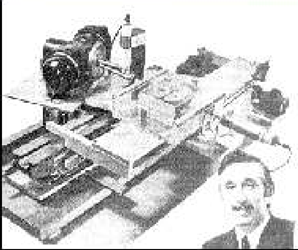

[2]

Gamma Ray Source: 28,000 measurements, 9 day collection, 2.5 hour recon, 2hour display.

X-ray source reduced collection to 9 hours. Clinical model took 18 sec

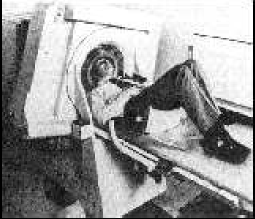

[1]

EMI-1, 1971:
Atkinson Morley Hospital, England

# Allan M. Cormack

1924-1998, narozen v Johannesburgu

# Tomography modalities

- x-rays — CT
- gamma rays — PET, SPECT
- light — optical tomography
- RF waves — MRI
- DC — electric impedance tomography
- ultrasound — ultrasound tomography

# Základní princip CT

***CT vytváří obraz těla pacienta jako sérii tomografických sekcí (řezů). Každý řez je vytvořen matematickou rekonstrukcí předmětu ze znalosti průmětů (projekcí) předmětu do různých směrů.***

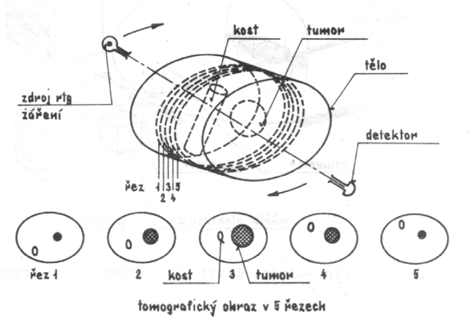

# Základní princip CT

**Jednotlivé řezy objektu musí být rozděleny do sítě malých objemových elementů (voxels) se čtvercovou základnou a s konstantní hodnotou útlumu.**

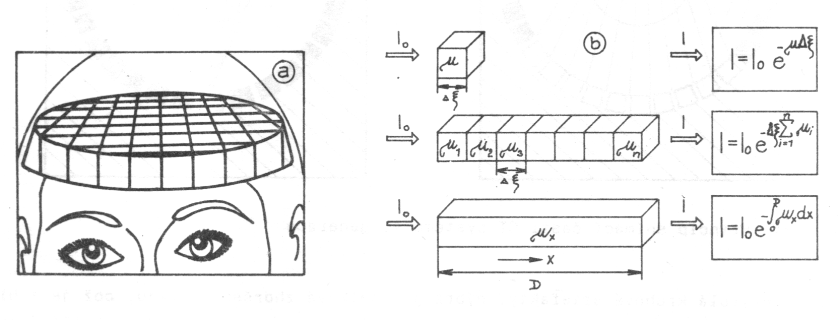

# Základní fyzikální princip CT

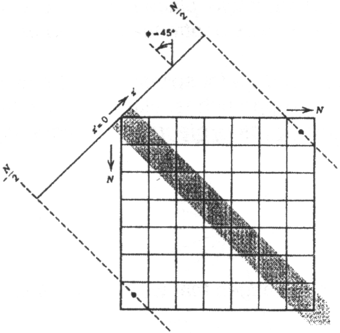


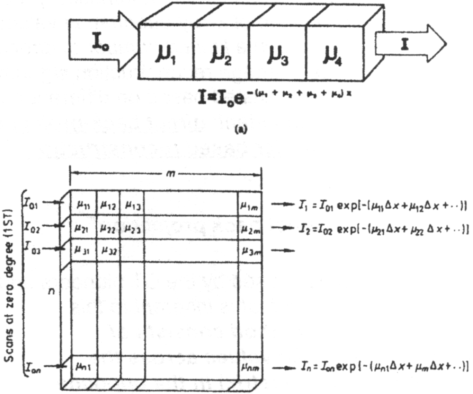

# CT systémy 1. generace

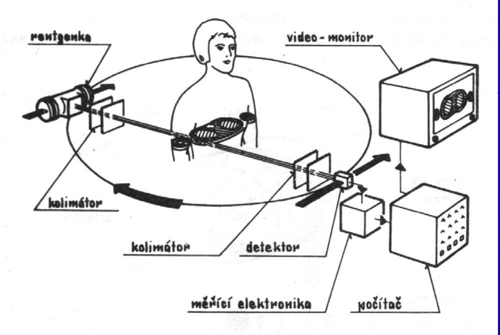


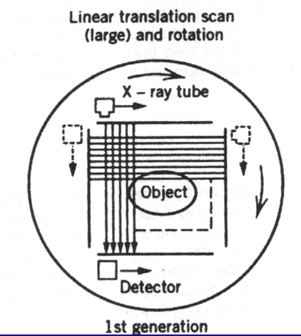

# CT systémy 2. generace

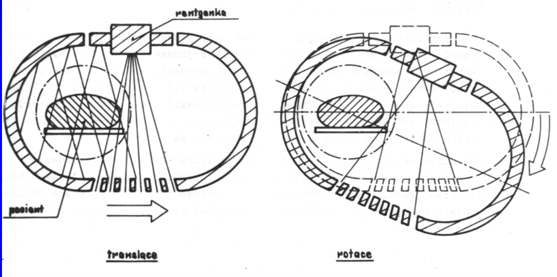


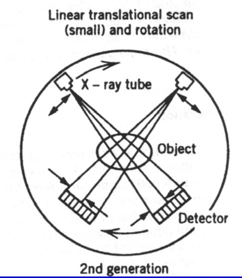

# CT systémy 3. generace

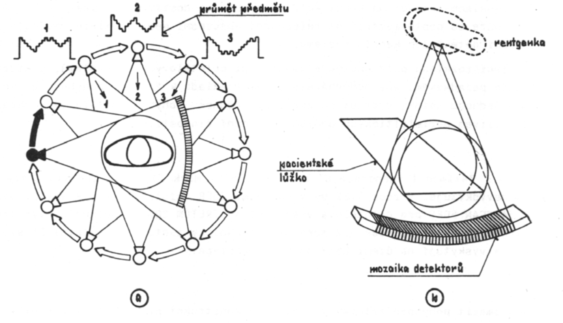


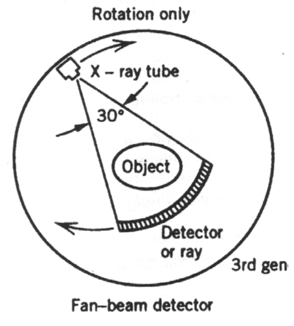


asi nejčastěji používané

# CT systémy 4. generace

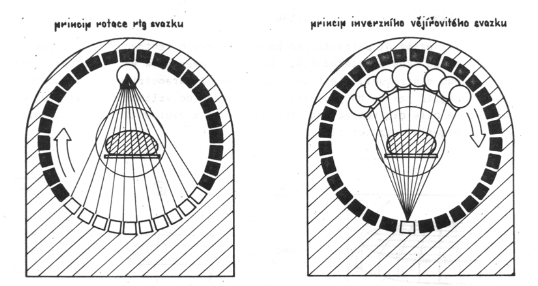


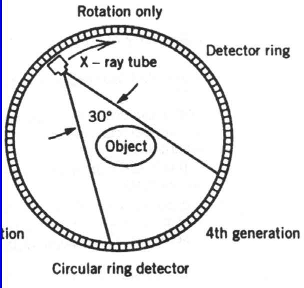


Rotuje jen zdroj, detektory stabilni

# „Utvrzování svazku“ (beam hardening)

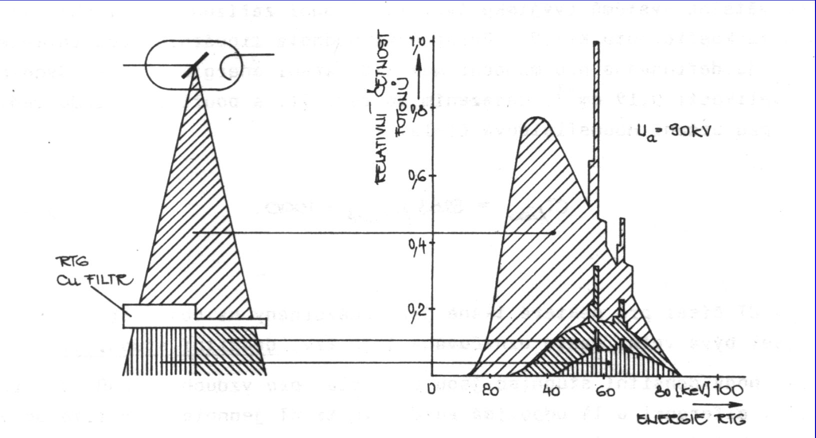

# „Utvrzování svazku“ (beam hardening)

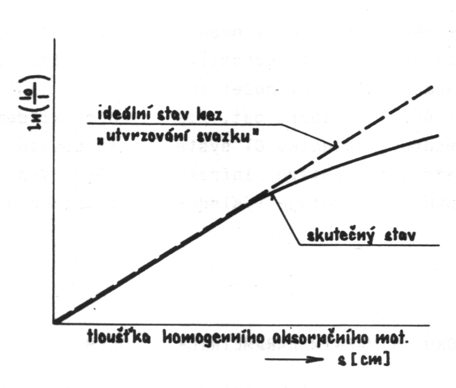

# CT číslo - Haunsfieldovo číslo (HU)

**Je vyjádřením kvantitativního hodnocení absorbčních vlastností tkáně.**

$$CT = K\,.\,\frac{{}_{\text{tkáně}} - {}_{\text{vody}}}{{}_{\text{vody}}}$$

$$K = 1000$$

$${}_{\text{vody}} = 0{,}19\ \text{cm}^{-1}$$

**Měřeno monochromatickým zářením 73 keV.**

$$CT = 5263\ {}_{\text{tkáně}} - 1000$$

**stupnice CT čísel = denzitní stupnice**

**rozsah od -1000 až zhruba +1000, pro vzduch -1000, pro vodu 0**

# CT číslo - Haunsfieldovo číslo (HU)

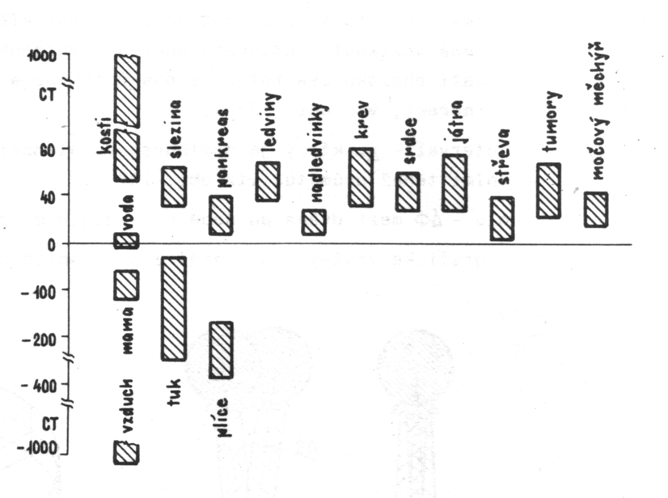

# Generace, zpracování a detekce radiačního signálu CT systémů

CT systémy 2. generace
(několik detektorů)

- pomalé a rychlé systémy
- sendvičový a lamelový kolimátor

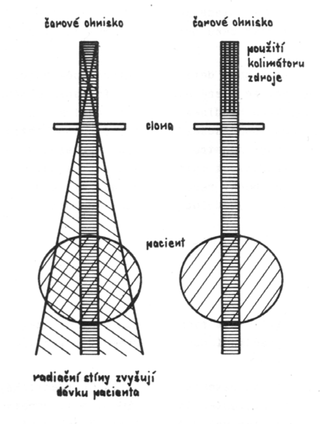

# Generace, zpracování a detekce radiačního signálu CT systémů

## Detektory

**scintilační detektor (krystal) + fotonásobič**

**ionizační komory plněné plynem (xenon)**

**scintilační detektor (krystal) + fotodioda (fototranzistor)**

Flat-panel detector (FPD)
Thin-film transistor (TFT) array

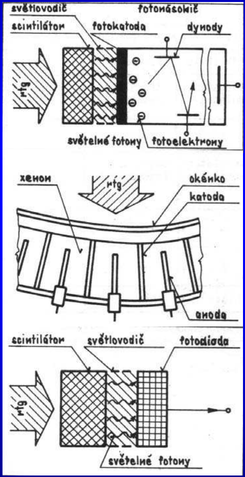


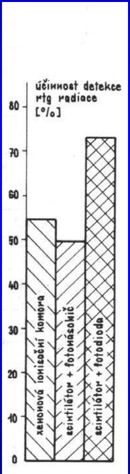

# Základní principy rekonstrukce obrazu

$o(\xi,\eta)$ **denzitní funkce = předmětová funkce lin. součinitel zeslabení**

$(\xi,\eta)$ **původní souř.**

$\Phi$ **snímací úhel**

$\xi'$ **rotovaná souř.**

$\eta'$ **rotovaná souř.**

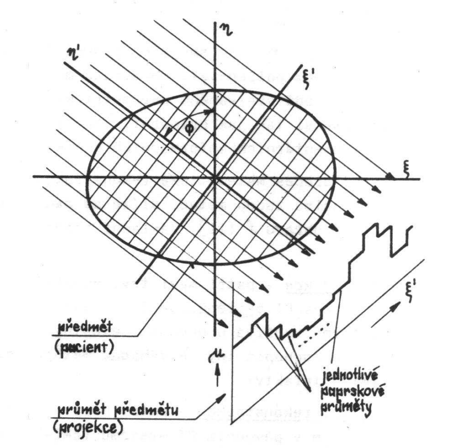


$p(\xi',\Phi)$ **paprskový součet či průmět**

# Základní principy rekonstrukce obrazu

$$\mathrm{p}(\xi', \Phi) = \int \mathrm{o}(\xi, \eta)\, \mathrm{d}\eta' \qquad \mathrm{I} = \mathrm{I}_0 \exp\left[ -\int \quad (\xi, \eta)\, d\eta \right]$$

$$\mathrm{o}(\xi, \eta) \approx \quad (\xi, \eta)$$

$$\boxed{\mathrm{p}(\xi', \Phi) = -\ln \frac{\mathrm{I}_0}{\mathrm{I}}}$$

$$\boxed{\xi' = \xi.\cos\Phi + \eta.\sin\Phi} \qquad \xi = \xi'.\cos\Phi - \eta.\sin\Phi$$

$$\eta' = -\xi.\sin\Phi + \eta.\cos\Phi \qquad \eta = \xi'.\sin\Phi + \eta.\cos\Phi$$

# Radon transform

Projection in polar coordinates:

$$P_\varphi(\xi') = \mathscr{R}\left[o(\xi,\eta)\right]$$
$$P_\varphi(\xi') = \int_L o(\xi,\eta)\mathrm{d}l$$

along the line $L$ defined by $\varphi$ a $\xi'$:

$$\xi' = \xi\cos\varphi + \eta\sin\varphi$$

Equivalently

$$P_\varphi(\xi') = \int o(\xi'\cos\varphi - \eta'\sin\varphi, \xi'\sin\varphi + \eta'\cos\varphi)\mathrm{d}\eta'$$

# Radonova transformace

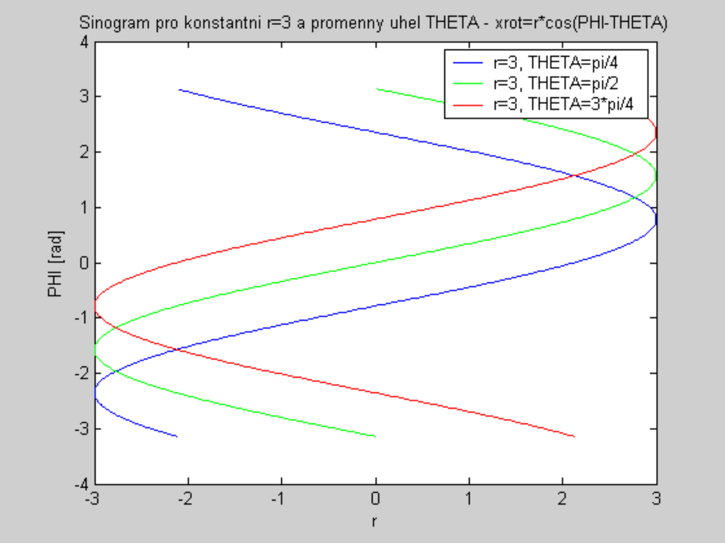

# Radonova transformace

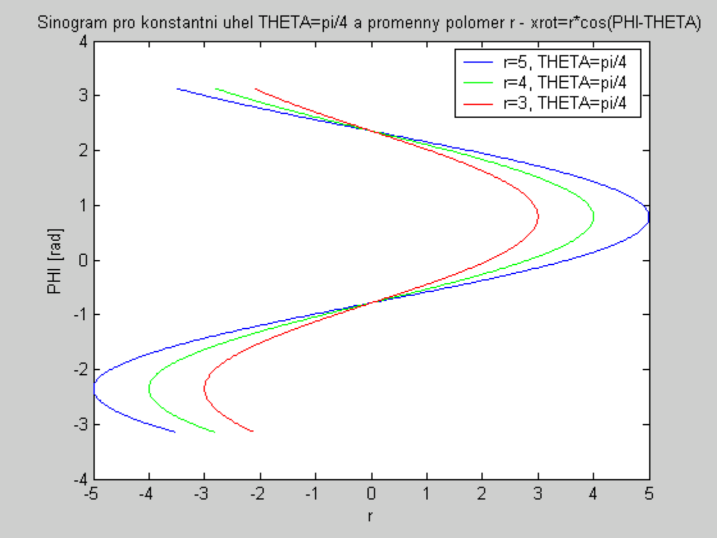

# Radonova transformace

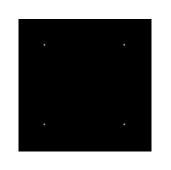

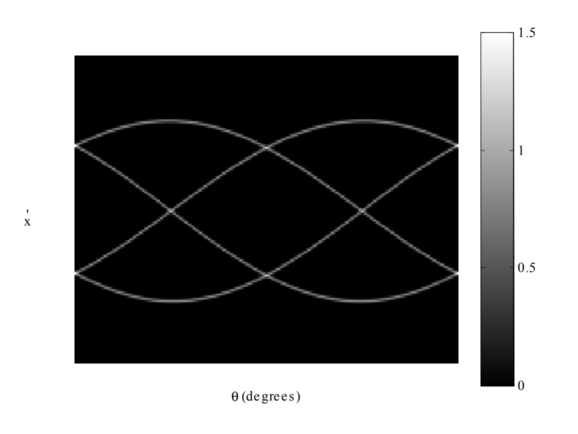

# Radonova transformace

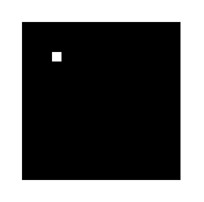

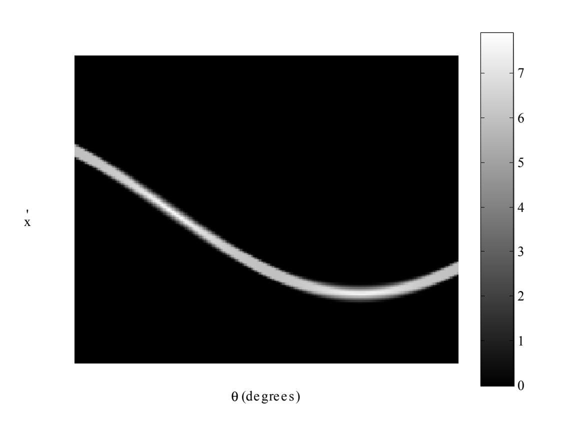

# Radonova transformace

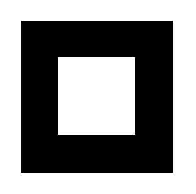

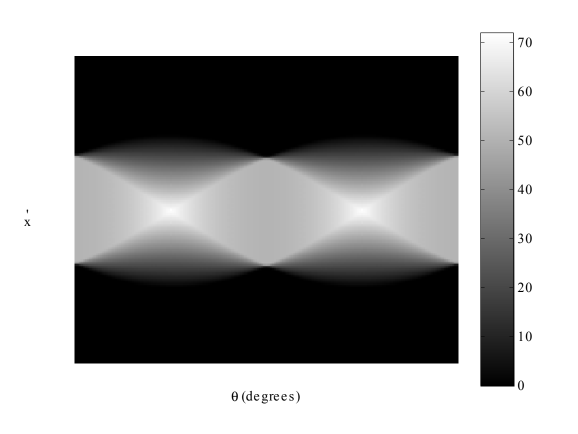

# Radonova transformace

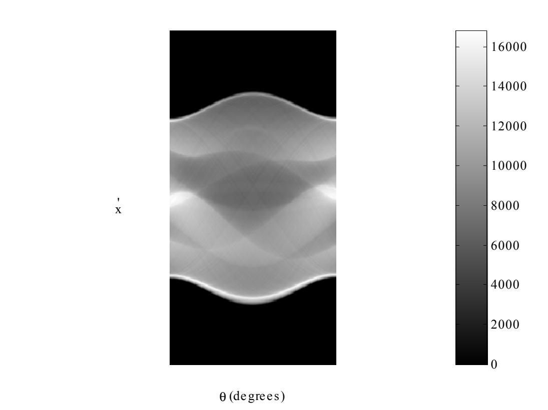


Shepp-Logan fantom

# Radonova transformace

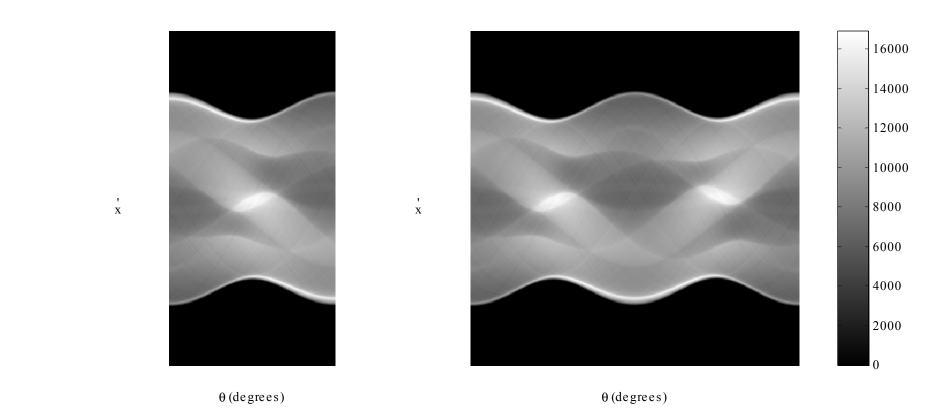


Periodicity RT vůči úhlu

# Reconstruction methods

- *Backprojection*
- *Fourier reconstruction*
- Filtered backprojection
- Algebraic reconstruction (iterative)

# Přímá zpětná projekce

$$\mathrm{i}(x,y)=\sum_{j=1}^{m}\mathrm{p}\left(\xi',\Phi_{\mathrm{j}}\right)\Delta\Phi$$

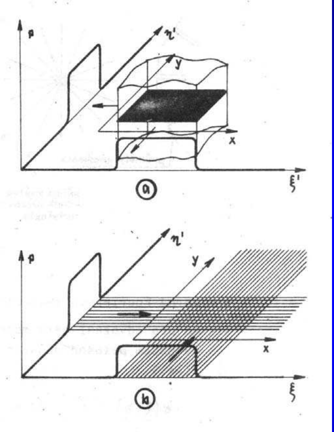


$\Phi_{\mathrm{j}}$ **j-tý projekční úhel**

$\Delta\Phi$ **úhlový přírůstek mezi projekcemi**

$m$ **počet projekcí**

$$\mathrm{i}(x,y)=\sum_{j=1}^{m}\mathrm{p}\left(\left(x.\cos\Phi_{\mathrm{j}}+y.\sin\Phi_{\mathrm{j}}\right),\Phi_{\mathrm{j}}\right)\Delta\Phi$$

# Přímá zpětná projekce - hvězdicový artefakt

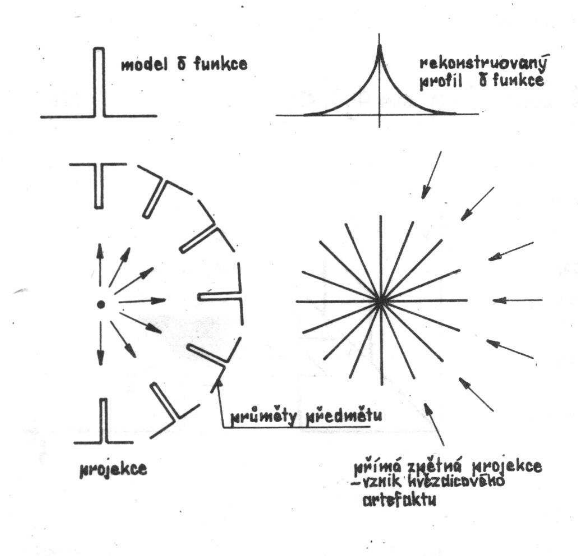

# Central slice theorem

Projection Theorem, Věta o centrálním řezu)

$$P_\varphi(\xi') = \int o(\xi' \cos\varphi - \eta' \sin\varphi, \xi' \sin\varphi + \eta' \cos\varphi) \mathrm{d}\eta'$$

Fourier transform of the Radon transform by $\xi'$:

$$\begin{aligned}\mathscr{F}\left\{\mathscr{R}\left[o(\xi,\eta)\right]\right\} = \mathscr{F}\left\{P_\varphi(\xi')\right\} = \hat{P}_\varphi(\omega) &= \int P_\varphi(\xi') \mathrm{e}^{-2\pi j\omega\xi'} \mathrm{d}\xi' \\ &= \iint o(\xi' \cos\varphi - \eta' \sin\varphi, \xi' \sin\varphi + \eta' \cos\varphi) \mathrm{e}^{-2\pi j\omega\xi'} \mathrm{d}\xi' \mathrm{d}\eta'\end{aligned}$$

Substitution $(\xi', \eta') \to (\xi, \eta)$:

$$\hat{P}_\varphi(\omega) = \int o(\xi,\eta) \mathrm{e}^{-2\pi j\omega(\xi\cos\varphi + \eta\sin\varphi)} \mathrm{d}\xi \mathrm{d}\eta$$

# Central slice theorem

$$\hat{P}_{\varphi}(\omega) = \int o(\xi,\eta) \mathrm{e}^{-2\pi j \omega(\xi\cos\varphi + \eta\sin\varphi)} \mathrm{d}\xi \mathrm{d}\eta$$

Denote $u = \omega\cos\varphi \quad v = \omega\sin\varphi$

$$\hat{P}(u,v) = \int o(\xi,\eta) \mathrm{e}^{-2\pi j(\xi u + \eta v)} \mathrm{d}\xi \mathrm{d}\eta$$

and therefore

$$\begin{aligned} \hat{P}(u,v) &= \mathscr{F}\left\{o(\xi,\eta)\right\} \\ \hat{P}_{\varphi}(\omega) &= \mathscr{F}\left\{o(\xi,\eta)\right\}(\omega\cos\varphi, \omega\sin\varphi) = \hat{o}(\omega\cos\varphi, \omega\sin\varphi) \end{aligned}$$

# Central slice theorem

$$\hat{P}(u, v) = \mathscr{F}\{o(\xi, \eta)\}$$
$$\hat{P}_\varphi(\omega) = \mathscr{F}\{o(\xi, \eta)\}(\omega \cos\varphi, \omega \sin\varphi) = \hat{o}(\omega \cos\varphi, \omega \sin\varphi)$$

Slice of the 2D Fourier transform of the image $o$ at angle $\varphi$ is the 1D Fourier transform of the projection $P_\varphi$ of the same image $o$.

# Analytická rekonstrukce - 2D FT

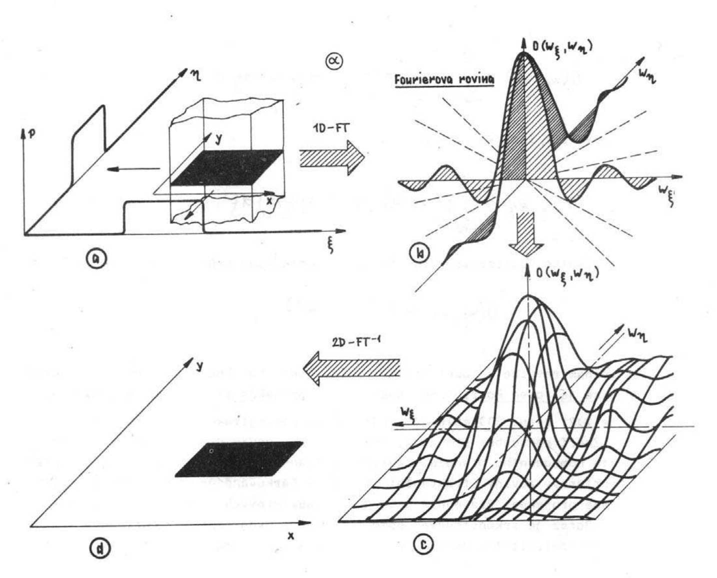

# Analytická rekonstrukce - 2D FT

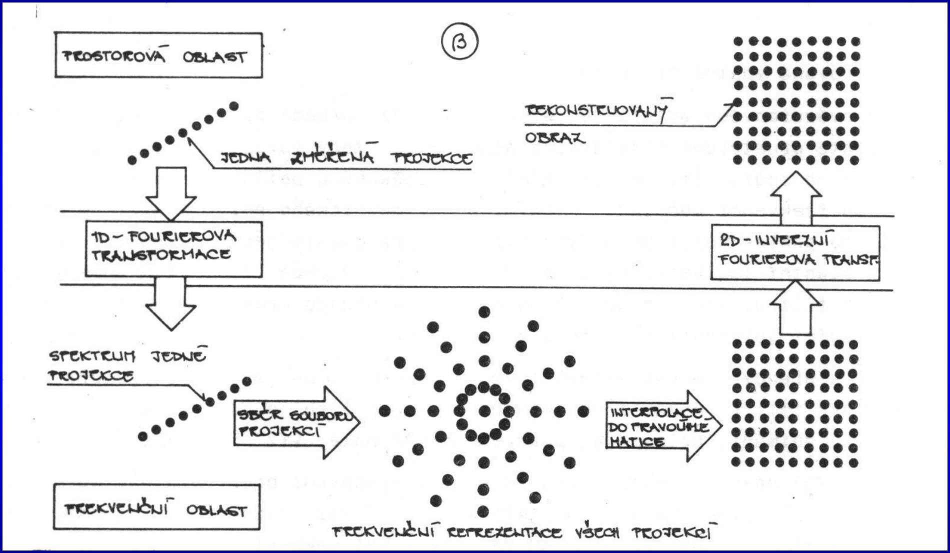

# Inverse Radonova transform

From the Fourier slice theorem:

$$\hat{P}(u,v) = \mathscr{F}\left\{o(\xi,\eta)\right\}$$

$$o(\xi,\eta) = \mathscr{F}^{-1}\left\{\hat{P}(u,v)\right\} = \int_{-\infty}^{\infty}\int_{-\infty}^{\infty} \hat{P}(u,v)\mathrm{e}^{2\pi j(\xi u+\eta v)}\mathrm{d}u\mathrm{d}v$$

Polar coordinates $u = \omega\cos\varphi, \quad v = \omega\sin\varphi$:

$$o(\xi,\eta) = \int_{0}^{\pi}\int_{-\infty}^{\infty} \hat{P}_{\varphi}(\omega)\mathrm{e}^{2\pi j\omega(\xi\cos\varphi+\eta\sin\varphi)}|\omega|\mathrm{d}\omega\mathrm{d}\varphi$$

where $|\omega|$ is the Jacobian (determinant).

# Inverse Radonova transform

$$o(\xi, \eta) = \int_{0}^{\pi} \int_{-\infty}^{\infty} \hat{P}_{\varphi}(\omega) \mathrm{e}^{2\pi j \omega (\xi \cos\varphi + \eta \sin\varphi)} |\omega| \mathrm{d}\omega \mathrm{d}\varphi$$

can be written as

$$o(\xi, \eta) = \int_{0}^{\pi} Q_{\varphi}(\underbrace{\xi \cos\varphi + \eta \sin\varphi}_{\xi'}) \mathrm{d}\varphi$$

$$Q_{\varphi}(\xi') = \int_{-\infty}^{\infty} \hat{P}_{\varphi}(\omega) \mathrm{e}^{2\pi j \omega \xi'} |\omega| \mathrm{d}\omega$$

where $Q_{\varphi}(\xi')$ is a modified projection

# Inverse Radonova transform

$$o(\xi,\eta) = \int_0^\pi Q_\varphi(\xi')\mathrm{d}\varphi$$

$$Q_\varphi(\xi') = \int_{-\infty}^{\infty} \hat{P}_\varphi(\omega)\mathrm{e}^{2\pi j\omega\xi'}|\omega|\mathrm{d}\omega$$

$$Q_\varphi(\xi') = \mathscr{F}^{-1}\left\{|\omega|\hat{P}_\varphi(\omega)\right\} = \mathscr{F}^{-1}\left\{|\omega|\right\} * P_\varphi(\xi')$$

defining the exact inverse Radon transform

$$P_\varphi(\xi') = \mathscr{R}\big[o(\xi,\eta)\big]$$
$$o(\xi,\eta) = \mathscr{R}^{-1}\big[P_\varphi(\xi')\big]$$

# Filtered backprojection

## Filtrovaná zpětná projekce

- Filter all projections $P_\varphi(\xi')$ for all $\varphi$, get modified projections $Q_\varphi(\xi')$
- Backprojected modified projections and sum

$$
\begin{aligned}
o(\xi, \eta) &= \int\limits_0^\pi Q_\varphi(\xi') \mathrm{d}\varphi \\
Q_\varphi(\xi') &= h(t) * P_\varphi(\xi') = \mathscr{F}^{-1}\left\{H(\omega)\right\} * P_\varphi(\xi') \\
H(\omega) &= |\omega|
\end{aligned}
$$

# Practical implementation of filtered backprojection

- **Problem:** Ideal filter $H(\omega) = |\omega|$ amplifies noise
- **Solution 1:** Make $\hat{P}_\varphi(\omega)$ frequency limited.
  Ramakrishnan-Lakshiminaryanan $\longrightarrow$ Ram-Lak filter:

$$H(\omega) = \begin{cases} |\omega| & \text{if } |\omega| \leq \Omega \\ 0 & \textit{otherwise} \end{cases}$$

# Practical implementation of filtered backprojection

- **Problem:** Ideal filter $H(\omega) = |\omega|$ amplifies noise
- **Solution 1:** Make $\hat{P}_\varphi(\omega)$ frequency limited. Ramakrishnan-Lakshiminaryanan $\longrightarrow$ Ram-Lak filter:

$$H(\omega) = \begin{cases} |\omega| & \text{if } |\omega| \leq \Omega \\ 0 & \textit{otherwise} \end{cases}$$

- Ram-Lak filter causes artefacts (Gibbs). Many solutions (Hamming filter, Shepp-Logan filter). Typically Hamming has better SNR but lower resolution.

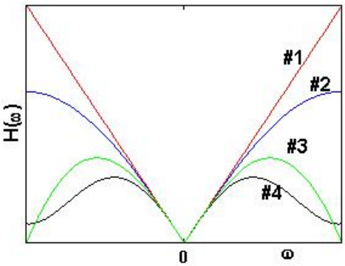

# Analytická rekonstrukce - filtrovaná ZP

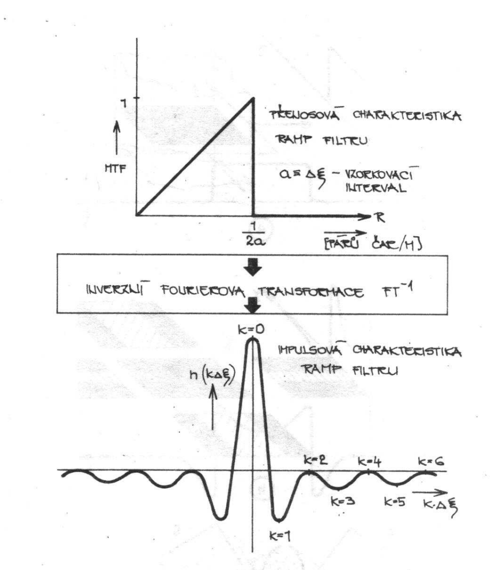


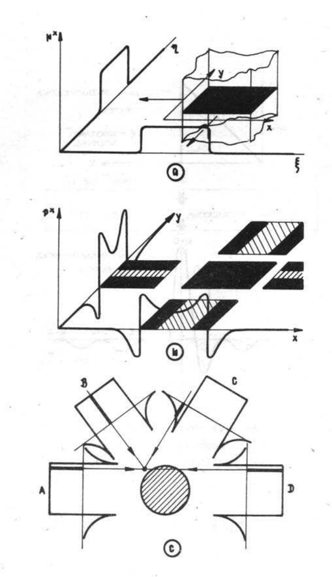

# Filtered backprojection

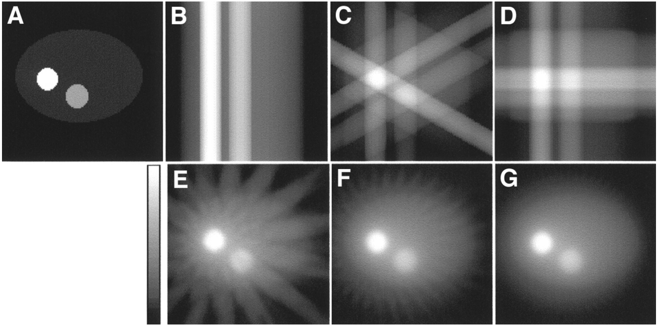


original image, 1,3, 4, 16, 32, a 64 projections

# Algebraic reconstruction

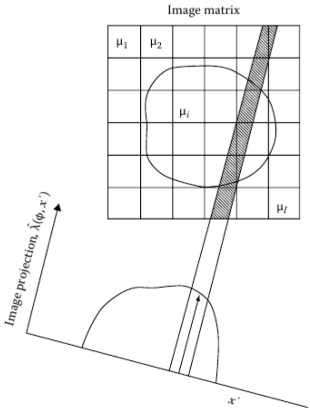


- setup equations, often linear

$$g_i = \sum_j w_{ij} f_j$$

where $f_j$ are pixel values, $g_i$ are projections

# Algebraic reconstruction

- setup equations, often linear

$$g_i = \sum_j w_{ij} f_j$$

where $f_j$ are pixel values, $g_i$ are projections

- We know $g_i$ and $w_{ij}$, solve for $f_i$
- Many unknowns ($10^5 \sim 10^6$), iterative methods
  - Compare measured projections and simulations
  - Correct pixel values to decrease the difference
  - Iterate until convergence

# Algebraic reconstruction

- setup equations, often linear

$$g_i = \sum_j w_{ij} f_j$$

  where $f_j$ are pixel values, $g_i$ are projections

- We know $g_i$ and $w_{ij}$, solve for $f_i$
- Many unknowns ($10^5 \sim 10^6$), iterative methods
  - Compare measured projections and simulations
  - Correct pixel values to decrease the difference
  - Iterate until convergence
- Methods:
  - algebraic reconstruction technique (ART)
  - simultaneous algebraic reconstruction technique (SART)
  - simultaneous iterative reconstruction (SIRT)
  - iterative least-squares technique (ILST)
  - multiplicative algebraic reconstruction technique (MART)

# Algebraic rekonstruction — advantages over FBP

- Better modeling of the physics — attenuation, resolution, noise
- Better handling of limited acquisition — restricted region, restricted angles
- Can use an image model
- Less apparent artifacts

# Iterativní rekonstrukce - ART

**ART – Algebraic Reconstruction Technique je jedním z mnoha použitých algoritmů, které se používají do současnosti. Existují dva základní typy ART:**

**- aditivní**

$$\widehat{f}_{ij}^{\,l} = \widehat{f}_{ij}^{\,l-1} + \frac{g_j - \sum_{i=1}^{N} \widehat{f}_{ij}^{\,l-1}}{N}$$

**- multiplikativní**

$$\widehat{f}_{ij}^{\,l} = \frac{g_j}{\sum_{i=1}^{N} \widehat{f}_{ij}^{\,l-1}} \widehat{f}_{ij}^{\,l-1}$$

# Iterativní rekonstrukce – ART pokračování

**kde:** $\widehat{f}_{ij}^{\,l}$ - **odhad hodnoty $i$-tého voxelu podél $j$-tého paprsku během $l$-té iterace,**

$g_j$ - **skutečný paprskový součet (data) podél $j$-tého paprsku,**

$N$ - **počet objemových elementů (voxelů) podél $j$-tého paprsku,**

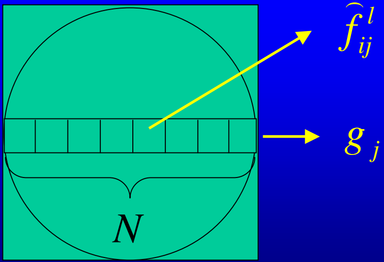

# Iterativní rekonstrukce – ART aditivní - příklad

- skutečná naměřená data (projekce a paprskové součty)

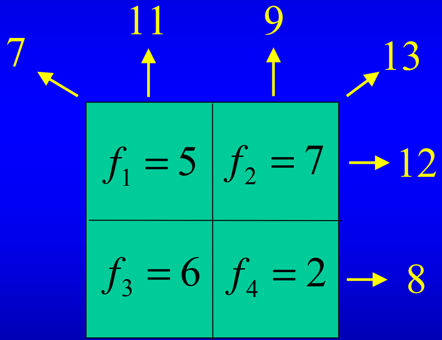

# Iterativní rekonstrukce – ART př. – pokrač.

**1/3**
**vertikální paprsky**

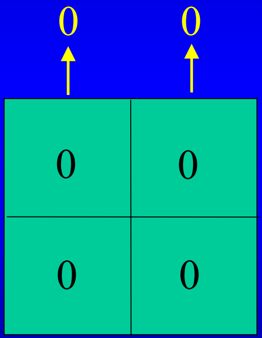


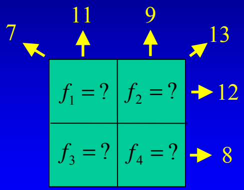


$$\hat{f}_1^{1/3} = \hat{f}_3^{1/3} = 0 + \frac{11 - 0}{2} = 5{,}5$$

$$\hat{f}_2^{1/3} = \hat{f}_4^{1/3} = 0 + \frac{9 - 0}{2} = 4{,}5$$

# Iterativní rekonstrukce – ART př. – pokrač.

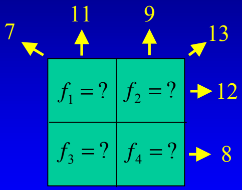


**2/3**
**horizontální paprsky**

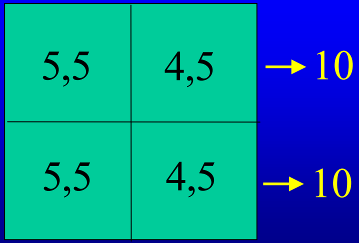


$$\hat{f}_1^{2/3} = 5,5 + \frac{12-10}{2} = 6,5$$

$$\hat{f}_2^{2/3} = 4,5 + \frac{12-10}{2} = 5,5$$

$$\hat{f}_3^{2/3} = 5,5 + \frac{8-10}{2} = 4,5$$

$$\hat{f}_4^{2/3} = 4,5 + \frac{8-10}{2} = 3,5$$

# Iterativní rekonstrukce – ART př. – pokrač.

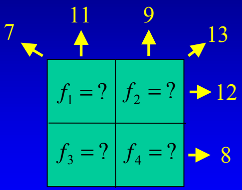


**3/3=1**

**diagonální paprsky**

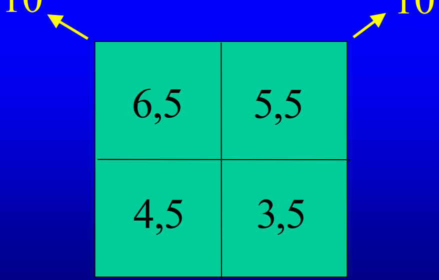


$$\left.\begin{array}{l}
\widehat{f}_1^{\,1} = 6{,}5 + \dfrac{7-10}{2} = 5 \\[2ex]
\widehat{f}_2^{\,1} = 5{,}5 + \dfrac{13-10}{2} = 7 \\[2ex]
\widehat{f}_3^{\,1} = 4{,}5 + \dfrac{13-10}{2} = 6 \\[2ex]
\widehat{f}_4^{\,1} = 3{,}5 + \dfrac{7-10}{2} = 2
\end{array}\right\} \textbf{viz orig. data}$$

Konvergence

# Electric processing — corrections

- Offset correction (zero signal at rest)
- Normalization correction (x-ray source intensity fluctuation)
- Sensitivity correction (inhomogeneous detectors and amplifiers)
- Geometric correction
- Beam hardening correction
- Cosine correction

# CT systémy 3. generace

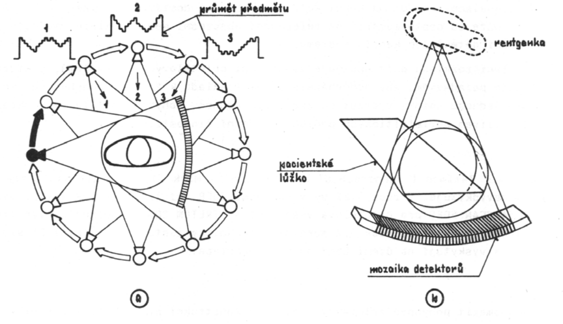


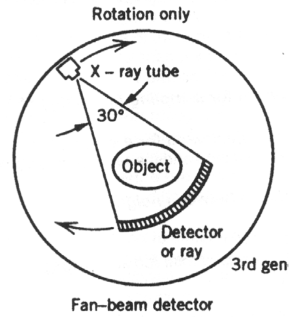


asi nejčastěji používané

# Fan-beam reconstruction

- Rays not parallel, not a Radon transform.
- Rebinning

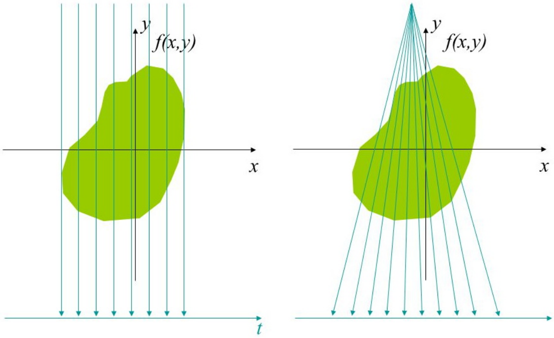


image courtesy of Gillian Henderson

# Fan-beam reconstruction

- Rays not parallel, not a Radon transform.
- Rebinning

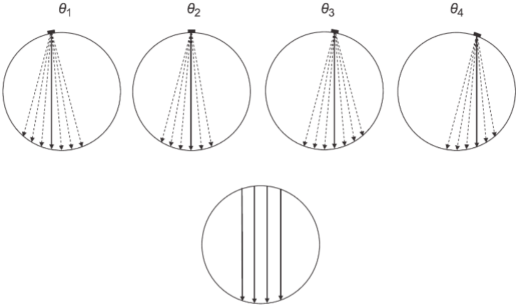


image courtesy of Jonathan Mamou and Yao Wang

# Fan-beam reconstruction (2)

- Rays not parallel, not a Radon transform.
- Exact algorithms:
  - Rebinning
  - filtered backprojection (Katsevich) — computational complexity, increased dose.
- Approximate algorithms: Modified filtered backprojection (quadratic cosine correction, $\cos\theta$). Feldkamp-Davis-Kress

# Fan-beam reconstruction (2)

- Rays not parallel, not a Radon transform.
- Exact algorithms:
  - Rebinning
  - filtered backprojection (Katsevich) — computational complexity, increased dose.
- Approximate algorithms: Modified filtered backprojection (quadratic cosine correction, $\cos\theta$). Feldkamp-Davis-Kress
- Algebraic reconstruction. Best quality but slow.

# 3D computed tomography

- Technical challenges: power, cooling
- Rotation method (slice by slice)
- Spiral/helix method

# Spiral method

- Acceleration: 10 min $\to$ 1 min

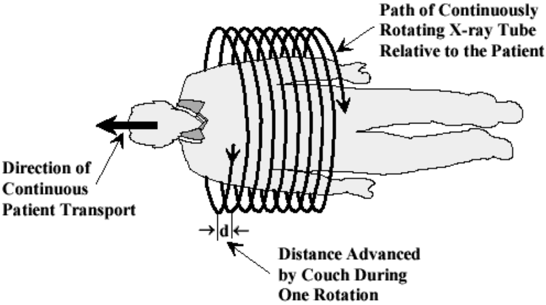

# Spiral method

- Acceleration: 10 min $\rightarrow$ 1 min
- *Pitch*:

$$P = \Delta l / d$$

$\Delta l$ bed shift per rotation, $d$ slice thickness.
Normally $0 < P < 2$. Overlap for $P < 1$. Typically $P = 1.5$.

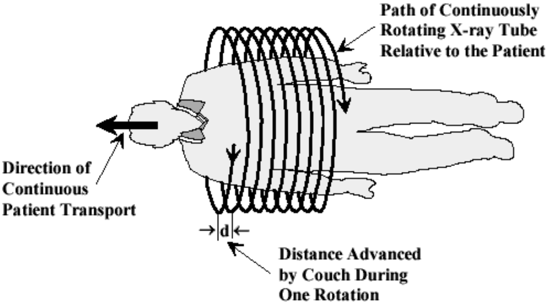

# Spiral method (2)

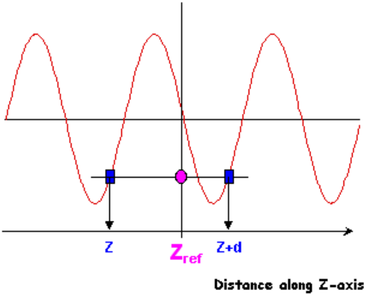


- Interpolation in $z$ axis
- Interpolation *wide* — 1 turn. Less noise, larger effective slice thickness.
- Interpolation *Slim* — $1/2$ turn, symmetry. More noise, smaller effective slice thickness.

# Multislice acquisition

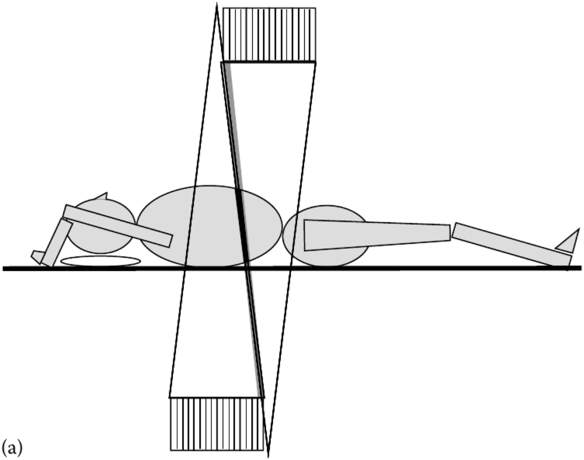

(a)

- Acceleration

# Multislice acquisition

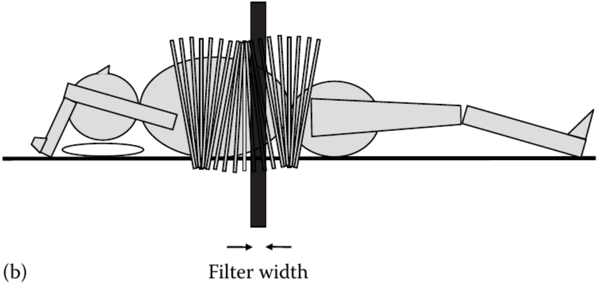

(b)

- Adaptive multi-plane reconstruction

# Radiation dose

- Absorbed dose $D$. $1\,\mathrm{Gy}$ (gray) $= 1\,\mathrm{J/kg}$ Before $1\,\mathrm{Gy} = 100\,\mathrm{rad}$
- Effective dose equivalent (dávkový ekvivalent)
  $H_\mathrm{E}$ [Sv] (sievert)

$$H_\mathrm{E} = \sum_i w_i H_i = \sum_i w_i c_i D_i$$

$H = cD$. Quality factor $c$ is 1 for X-rays and $\gamma$ rays, 10 for neutrons, 20 for $\alpha$ particles.

Coefficient $w$ is organ dependent: male/female glands 0.2, lungs 0.12, breast 0.1, stomach 0.12, thyroid gland 0.05, skin 0.01. $\sum w_i = 1$
Before $1\,\mathrm{Sv} = 100\,\mathrm{rem}$

# Radiation dose

- Absorbed dose $D$. 1 Gy (gray) = 1 J/kg Before 1 Gy = 100 rad
- Effective dose equivalent (dávkový ekvivalent)
  $H_\mathrm{E}$ [Sv] (sievert)

  $$H_\mathrm{E} = \sum_i w_i H_i = \sum_i w_i c_i D_i$$

  $H = cD$. Quality factor $c$ is 1 for X-rays and $\gamma$ rays, 10 for neutrons, 20 for $\alpha$ particles.

  Coefficient $w$ is organ dependent: male/female glands 0.2, lungs 0.12, breast 0.1, stomach 0.12, thyroid gland 0.05, skin 0.01. $\sum w_i = 1$
  Before 1 Sv = 100 rem
- Sum the doses

# Radiation dose

- Medical limit (USA) is 50 mSv/year (=limit for a person working with radiation in CR), corresponding to 1000 chest X-rays, or 15 head CTs, or 5 whole body CTs (1 CT$\approx$ 10 mSv).
- low-dose CT$\approx 2 \sim 5$ mSv, PET$\approx$ 25 mSv
- In CR radioactive background about 3 mSv/year (mainly radon), similar to USA. In Colorado (altitude $1500 \sim 4000$ m) about 4.5 mSv/year. Mean dose from medical imaging 0.3 mSv/year, about 3 long flights.

# Radiation dose

- Medical limit (USA) is 50 mSv/year (=limit for a person working with radiation in CR), corresponding to 1000 chest X-rays, or 15 head CTs, or 5 whole body CTs (1 CT$\approx$ 10 mSv).
- low-dose CT$\approx 2 \sim 5$ mSv, PET$\approx$ 25 mSv
- In CR radioactive background about 3 mSv/year (mainly radon), similar to USA. In Colorado (altitude $1500 \sim 4000$ m) about 4.5 mSv/year. Mean dose from medical imaging 0.3 mSv/year, about 3 long flights.
- cancer related death 20 %. 1 CT=10 mSv — relative increase by $10^{-3} \sim 10^{-4}$

# CT image quality

- Parameters:
  - Resolution (0.5 mm)
  - Contrast ($\delta H$, about $5 - 10$ HU.)
  - Detection threshold (about 1 mm at $\Delta H = 200$, 5 mm at $\Delta H = 5$).
  - Noise (SNR)
- Artifacts
  - Scanner defects, malfunctions, operator error
  - Metal parts (shadows)
  - Motion artifacts
  - Partial volume

# Artifact examples

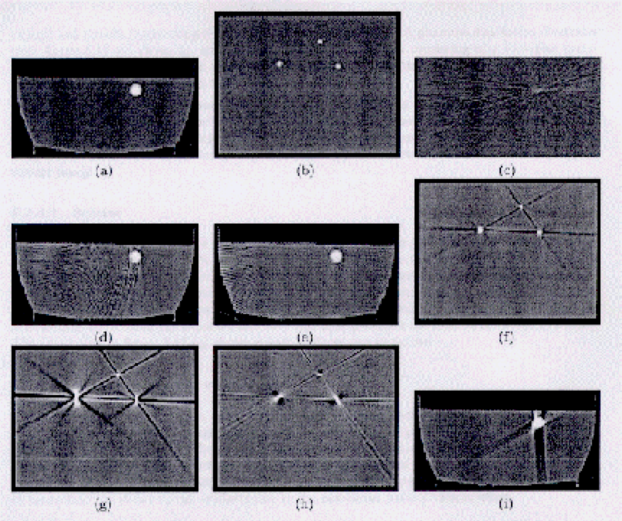


**Figure 2.19 Example of image artifacts:** (a) test phantom, (b) second phantom, (c) noise, (d) detector under-sampling, (e) view under-sampling, (f) beam hardening, (g) scatter, (h) nonlinear partial volume effect, and (i) object motion. (unpublished results)

# Clinical applications

- Lungs

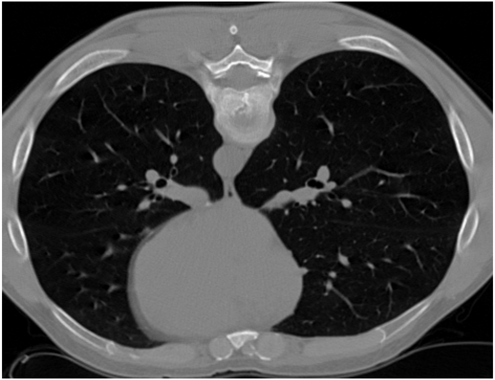

# Clinical applications

- Lungs

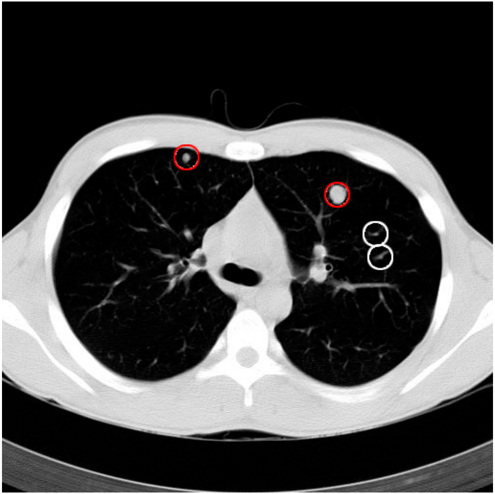

# Clinical applications

- Lungs
- Head

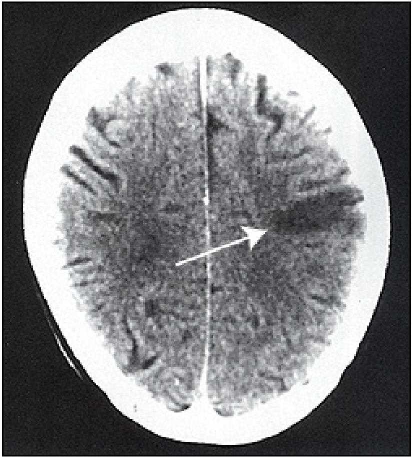

# Clinical applications

- Lungs
- Head

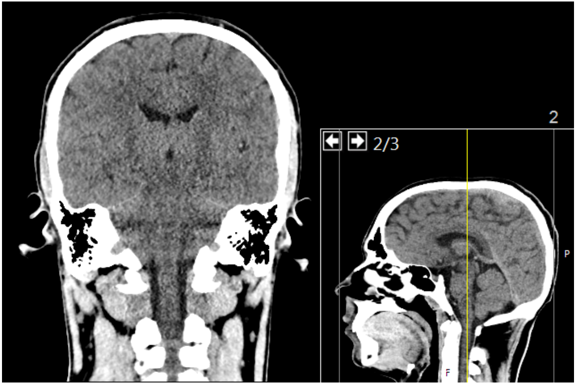

# Clinical applications

- Lungs
- Head

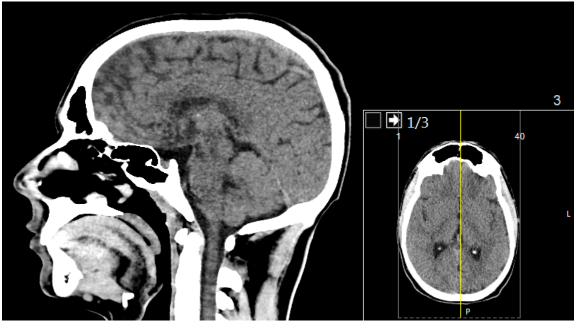

# Clinical applications

- Lungs
- Head
- Abdomen

# Computed tomography, conclusions

- Excellent spatial resolution
- 3D image
- Fast acquisition
- Weak soft tissue contrast (contrast agents available)
- Reconstruction algorithm
- Radiation dose